A Kinetic and Product Study of the Hydrolysis of $ClONO_2$ on Type Ia Polar Stratospheric Cloud Materials at 185 K

Stephen B. Barone,* Mark A. Zondlo, and Margaret A. Tolbert

Department of Chemistry and Biochemistry and the Cooperative Institute for Research in Environmental Sciences, University of Colorado, Boulder, Colorado 80309

Received: March 28, 1997; In Final Form: June 24, 1997[⊗]

A Knudsen cell reactor equipped with FTIR reflection−absorption spectroscopy (FTIR-RAS) has been used to study the hydrolysis of chlorine nitrate ($ClONO_2$) on thin nitric acid trihydrate (NAT) and nitric acid dihydrate (NAD) films. The reaction efficiencies and condensed-phase products have been measured for a variety of water partial pressures at 185 K. The reaction efficiencies for $ClONO_2$ hydrolysis on NAT and NAD were of similar magnitude and increased from $\gamma = 0.0004$ to $\gamma = 0.007$ as the water partial pressure was increased from 5×10^{-6} to 1.4×10^{-4} Torr. Although these values agree well with literature values at 90% relative humidity, significant differences are observed at lower relative humidities. Using our results at 185 K along with previous studies at 191 and 202 K, we suggest that this reaction may have a temperature dependence that is not currently addressed in atmospheric models. In the condensed phase, we observed the water dependence by the formation of progressively water-rich surface layers. The amount of water incorporated onto the NAT and NAD films increased with increasing relative humidity, suggesting that $ClONO_2$ hydrolysis occurs most efficiently on a water-rich hydrate surface. For water saturation ratios $S \geqslant 1.5$, nucleation and growth of crystalline ice was observed to occur in the aqueous HNO_3 surface layer on top of the reactant NAD and NAT films.

Introduction

Since the discovery of the Antarctic ozone hole in 1985, a large number of measurements in the laboratory and field have firmly established the critical role played by heterogeneous reactions in the chemistry of the lower stratosphere.[1−4] These reactions, occurring on the surfaces of polar stratospheric clouds (PSCs), convert stable chlorine reservoir species ($ClONO_2$ and HCl) into active chlorine which can catalytically destroy O_3. In addition, heterogeneous reactions result in a deactivation of nitrogen oxides via the formation of condensed-phase HNO_3 from less stable NO_y reservoirs ($ClONO_2$ and N_2O_5). One reaction that simultaneously leads to both Cl activation and NO_x sequestering is the hydrolysis of $ClONO_2$:

$$ClONO_2 + H_2O \rightarrow HOCl + HNO_3 \qquad (1)$$

Reaction 1 has been extensively studied and shown to proceed at a wide range of efficiencies on the various cloud surfaces likely to be present in the polar stratosphere. These surfaces include water ice, nitric acid trihydrate (NAT), nitric acid dihydrate (NAD), sulfuric acid tetrahydrate (SAT), and supercooled ternary solutions of $H_2SO_4/HNO_3/H_2O$.[5−12]

Previous investigations of reaction 1 on the various PSC surfaces focused on determining the rates of loss of reactants and formation of gas-phase products. These studies have clearly shown that reaction 1 proceeds very efficiently on water ice.[13,14] In contrast, reaction 1 has been shown to proceed somewhat less rapidly on the various acid hydrate surfaces likely present in the polar stratosphere (NAT, NAD, and SAT). The reaction efficiency on these hydrates also appears to be dependent on relative humidity with an increasing reaction efficiency at higher relative humidities.[5,6] In combination, these results have been interpreted to suggest that the availability of H_2O on the hydrate surface is a dominant factor in determining the rate of reaction 1 on PSCs.[15,16]

Although the rate of reaction 1 on model PSC surfaces has been extensively studied, there have been comparatively few investigations of the mechanism and condensed-phase products of this reaction.[14−19] In addition, previous studies relied on indirect methods of monitoring the reactant surfaces under investigation. Considering the pronounced dependence on H_2O availability, exact characterization of the reactant surface and bulk composition for temperatures and water pressures representative of the lower stratosphere is crucial for a complete understanding of this reaction.

The present study was undertaken to address the uncertainties mentioned above. To this end we have developed a new technique for studying heterogeneous reactions in which a Knudsen cell flow reactor is coupled to a surface sensitive probe consisting of FTIR-RAS. This technique allows for simultaneous real-time observations of the gas and condensed phases. In addition, this technique allows for accurate reactant film identification and characterization prior to exposure to reactant gases. We have studied reaction 1 on α-NAT, β-NAT, and NAD surfaces at 185 K and report both uptake efficiencies and product observations as a function of relative humidity.

Experimental Section

Apparatus. The reactive uptake of $ClONO_2$ on a variety of nitric acid hydrate surfaces was studied using a Knudsen cell flow reactor equipped with FTIR-RAS, a highly sensitive surface/bulk probe. The Knudsen cell reactor is very similar to those used in previous studies,[20,21] but modified to allow for FTIR-RAS measurements of the composition of the surface undergoing chemical reaction.

The apparatus consists of two stainless steel chambers connected by a butterfly valve as shown schematically in Figure 1. The upper chamber houses a circular metal substrate ($d =$ 9.14 cm), made of either optically flat aluminum or gold, on which thin films representative of polar stratospheric clouds are grown by vapor deposition. The substrate is cooled on the

[⊗] Abstract published in *Advance ACS Abstracts,* October 1, 1997.

S1089-5639(97)01107-9 CCC: $14.00

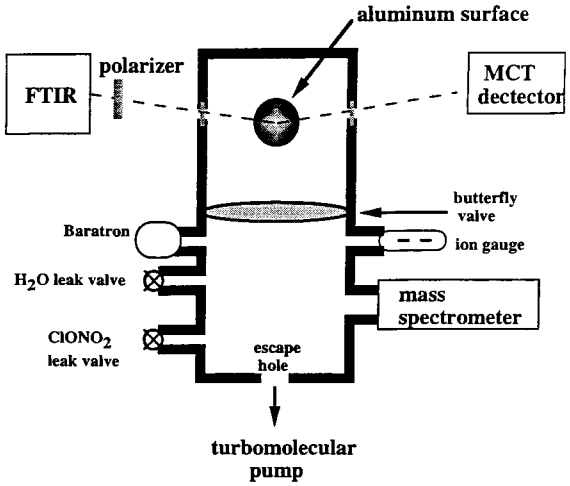

Figure 1. A schematic of the Knudsen/FTIR-RAS apparatus used in the present study.

backside by a temperature-controlled cryostat. The cryostat consists of a Kapton heater pressed between two aluminum supports. One of these supports is always kept in contact with a liquid nitrogen reservoir. The other aluminum support serves both as a thermal break to minimize any temperature gradients produced by the Kapton heater and as a mount onto which the substrate is directly attached by six evenly spaced screws. The temperature of the substrate is controlled by resistive heating. A differentially pumped sleeve houses the entire heating/cooling assembly to ensure that the only cold surface in the chamber is the metal substrate.

The temperature of the metal substrate is measured by copper−constantan thermocouples attached directly onto the surface using a thermally conductive epoxy. The surface temperature is also indirectly measured by determining the frost point vapor pressure of H_2O over a pure ice film as described by Middlebrook et al.[22] When no net loss or growth of the ice film is observed in the FTIR-RAS spectra, the corresponding H_2O partial pressure is used as the ice frost point. The thermocouple measurements always agreed within 2 K of the frost point temperature determined in this method. Our cryostat configuration allows for accurate temperature control over the range 90−400 K with a stability of ±0.1 K. The temperature gradient across the metal substrate is 0.2−0.5 K at 185 K as measured by the five thermocouples. The center of the substrate is the coldest location with slightly warmer temperatures toward the edge.

The lower chamber is coupled to a differentially pumped electron-impact ionization mass spectrometer, an ionization gauge, and a Baratron capacitance manometer to measure gas-phase partial pressures. Gases are introduced into the lower chamber via two precision leak valves and escape effusively through a small diameter hole upstream of the turbomolecular pump. The ionization gauges were routinely calibrated to the Baratron capacitance manometer.

FTIR-RAS Measurements of Condensed Phase. As shown schematically in Figure 1, characterization of reactant films and detection of condensed-phased products were performed in situ by reflection−absorption infrared spectroscopy at grazing angles. FTIR-RAS has been used in previous surface studies of heterogeneous atmospheric chemistry and shown to provide a sensitive means for detecting condensed-phase species such as $ClONO_2$ and H_2O.[18] Briefly, infrared radiation from a Nicolet 550 Magna FTIR spectrometer (silicon carbide source) was passed through a Molectron wire-grid polarizer to select only light polarized parallel to the plane of incidence. The infrared beam was then focused by a parabolic mirror onto the metal substrate at near grazing angles of incidence (≈84° from the surface normal). The reflected beam was collected by an ellipsoidal mirror and focused onto a liquid nitrogen-cooled HgCdTe detector. Typically, infrared spectra were collected over the range 4000−650 cm^{-1} at 10 s intervals and consisted of the coaddition of 64 scans at a resolution of 16 cm^{-1}.

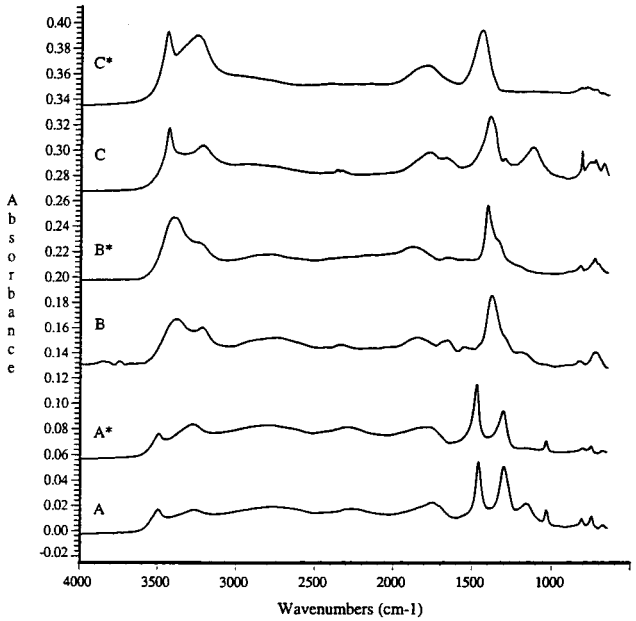

Figure 2. FTIR-RAS spectra of thin (A) NAD, (B) β-NAT, and (C) α-NAT films on an aluminum substrate at 185 K. Calculated FTIR-RAS spectra using optical constants from Toon et al.[25] are also shown for comparison and are designated by the * symbol.

Reactant NAD, β-NAT, and α-NAT films were formed by codepositing $ClONO_2$ and H_2O at 150 K and annealing the resulting films to 185 K at a rate of 10 K min^{-1}. In the presence of condensed-phase H_2O from codeposition, $ClONO_2$ rapidly converts to HNO_3. Thus, this technique is very similar to codeposition of HNO_3 and H_2O. Indeed, the reflection−absorption spectra of the resulting films at 150 K were identical with previously reported spectra of amorphous films of H_2O/HNO_3 ranging from 2:1 to 4:1 in composition.[23,24] Crystallization to NAT and NAD was observed to occur at temperatures between 170 and 185 K. β-NAT and NAD films were also prepared directly by codeposition of $ClONO_2$ and H_2O at 185 K. In this method, the infrared spectra indicated that codeposition initially resulted in supercooled liquids containing both HNO_3 and H_2O which, upon pumping, rapidly (t < 2 min) crystallized to β-NAT or NAD. For both methods NAD was formed by the crystallization of ≈2:1 H_2O:HNO_3 amorphous films, while NAT resulted from the crystallization of ≈3:1 H_2O:HNO_3 mixtures.

Identification of the NAT and NAD films was made by comparison with previously reported infrared spectra[23,24] and by calculations discussed below using infrared optical constants from Toon et al.[25] Figure 2 shows typical FTIR-RAS spectra of the thin NAD and NAT films used in the present study. The FTIR-RAS spectra shown in Figure 2 are very similar to transmission spectra reported in the literature; however, slight shifts in the peak positions and changes in relative intensities are noticeable.[23,24]

To further characterize our obtained FTIR-RAS spectra, we have calculated FTIR-RAS spectra for the thin nitric acid hydrate films using infrared optical constants from Toon et al.[25] and the equations given by Greenler[26] to describe infrared spectra obtained from grazing angle reflection off a metal surface. Figure 2 shows the calculated spectra (indicated by *) of 10 nm thick NAD and NAT films under the conditions of our experiment, i.e., light incident 84° from surface normal and films

grown on an aluminum substrate. As shown in Figure 2, it is clear that our observed NAT and NAD spectra are generally in good agreement with the calculated spectra. The most pronounced difference between calculated and observed spectra is the appearance of a peak at 1130 cm^{-1} in our experimental α-NAT and NAD spectra. The absorption at 1130 cm^{-1} has been previously reported in the infrared spectra of a stream of α-NAT aerosol formed at $T = 155$ K.[27] Although Richwine et al. attribute the appearance of the 1130 cm^{-1} feature to differences in aerosol and thin-film NAT lattice structures, the spectra obtained in the present study and results of Tisdale et al.[28] suggest the 1130 cm^{-1} absorption is related to crystallization of α-NAT and NAD at low temperatures. Indeed, to avoid the contamination of our α-NAT films with β-NAT, α-NAT films were always formed at lower temperatures ($T < 180$ K). The peak positions of the FTIR-RAS spectra of NAT and NAD films also agree with those reported in previous FTIR-RAS experiments; however, the observed relative peak intensities differ considerably.[29] These differences may be a result of different film preparation methods used in the present study or differences in the extent of polycrystallinity of the films investigated.

While the FTIR-RAS technique yields accurate information on composition and phase, exact characterization of film thickness is not possible with FTIR-RAS alone. Film thicknesses were thus estimated from deposition rates assuming that the crystal lattice spacing and thickness of NAT and NAD are similar to that of hexagonal H_2O ice (10^{15} sites cm^{-2} and 7 Å per bilayer)[30] and that deposition rates were constant across the entire substrate surface. From this we estimate our reactant films were in the range ≈5−50 nm thick. The integrated absorbance of the OH and nitrate bands of our NAT and NAD spectra varied linearly with film thickness over the range of those used in this study.

The FTIR-RAS spectra of our thin β-NAT and NAD reactant films were observed to be constant for long periods of time at 185 K. In contrast, α-NAT reactant films were observed to slowly convert to β-NAT at 185 K. Therefore, all kinetic studies of α-NAT surfaces at 185 K were compromised by the slow buildup of β-NAT during exposure to $ClONO_2$.

Determination of Reaction Efficiency. The reaction efficiency, γ, is defined as the fraction of molecular collisions with a surface that leads to reactive loss. The reaction efficiency of $ClONO_2$ on various nitric acid hydrate surfaces was determined by measuring the first-order loss rate resulting from uptake to the surface relative to its loss rate via effusion through the pump-out hole. The loss rate via effusion can be calculated for conditions of molecular flow; hence, absolute reaction efficiencies were obtained.

The rate of gaseous effusion out of the chamber for a known pressure of gas can be accurately calculated with knowledge of the gas pressure and effective hole area. However, because the hole is actually a cylinder rather than a perfect disk, the effective area is slightly smaller than the geometric area of the hole. The effective area of the hole was calibrated by measuring the chamber pressures for given flows of N_2 and He.[8] Flows of $(1.0-20) \times 10^{16}$ molecules s^{-1} were introduced to the chamber from a fixed volume reservoir while monitoring total pressure of the chamber, $(1-50) \times 10^{-4}$ Torr. The flows into the chamber were quantified by measuring the decrease in fixed volume line pressure as a function of time resulting from flow into the reaction chamber. The decrease in line pressure was monitored using differential pressure transducer calibrated to an absolute scale with a Baratron capacitance manometer.

The flow (F) of molecules into the chamber under conditions of molecular flow can be directly related to the area of the hole (A_h) and chamber pressure (P) by the following relationship:

$$F = (PA_h)/(2\pi mkT)^{0.5} \quad \text{(I)}$$

The slope of a plot of molecular flow rate versus chamber pressure yielded an effective hole area of $A_h = 0.17$ cm^2. This value was independent of the calibration gas used (N_2 or He). As expected, the effective hole area is slightly less than the geometric area of the hole (0.196 cm^2).

To obtain reaction efficiencies, the following methodology was used. Initially, $ClONO_2$ is flowed into the lower chamber. The only loss mechanism under these conditions is effusion through the 0.17 cm^2 hole. Hence, the steady-state concentration of $ClONO_2$ is given by

$$\{ClONO_2\}_{ss1} = F/(k_h V_1) \quad \text{(II)}$$

where F is the flow of $ClONO_2$ into the chamber (molecules s^{-1}), k_h (s^{-1}) is the first-order lost rate via effusion, and V_1 is the volume of the lower chamber. Under molecular flow conditions, the first-order effusive loss rate of $ClONO_2$ can be expressed as

$$k_h = (cA_h)/(4V_1) \quad \text{(III)}$$

where c is the average molecular velocity. Upon opening the butterfly valve which separates the upper and lower chambers, the flow of $ClONO_2$ is exposed to the reactant surface which can also act as a loss mechanism for $ClONO_2$. The new steady-state concentration of $ClONO_2$ is given by a similar equation to (II):

$$\{ClONO_2\}_{ss2} = F/((k_h + k_s)V_2) \quad \text{(IV)}$$

where k_s is the first-order loss rate due to reaction with the surface and V_2 is the combined volumes of the upper and lower chambers. The first-order losses to the surface and through the escape hole are given by the following expressions:

$$k_h = (cA_h)/(4V_2) \quad \text{(V)}$$

$$k_s = \gamma(cA_s)/(4V_2) \quad \text{(VI)}$$

where γ is the reaction efficiency and A_s is the area of the thin-film surface undergoing reaction. The ratio of the steady-state concentrations before and after exposure to the reactant surface can be related to the reaction efficiency by

$$\frac{[ClONO_2]_{ss1}}{[ClONO_2]_{ss2}} = \frac{(k_h + k_s)V_2}{(k_h)V_1} = \frac{A_h + \gamma A_s}{A_h} \quad \text{(VII)}$$

Solving for γ yields

$$\gamma = \frac{A_h}{A_s}\left(\frac{[ClONO_2]_{ss1} - [ClONO_2]_{ss2}}{[ClONO_2]_{ss2}}\right) = \frac{A_h}{A_s}\left(\frac{I_0 - I}{I}\right) \quad \text{(VIII)}$$

Thus, the reaction efficiency can be easily calculated by measuring the mass spectrometer signals of $ClONO_2$ before (I_0) and after (I) exposing the gas to the reaction surface and assuming the mass spectrometer signal varies linearly with concentration.

The range of reaction efficiencies that can be measured by our present design is determined by the ratio of the areas of the substrate surface to the escape hole. The upper limit of reaction efficiencies measurable by the current dimensions of our Knudsen cell reactor was determined by measuring the uptake of H_2O on ice at 120 K where it is known that water has a

sticking coefficient of unity.[31] Water deposition experiments at 120 K yielded an upper limit of $\gamma \geq 0.02$. The lower limit of $\gamma \leq 0.0002$ is determined by the uncertainty involved with subtracting off background loss of $ClONO_2$ to the reactor walls. Thus, we conclude that the present configuration allows for accurate measurement of reaction efficiencies in the range $(2-200) \times 10^{-4}$.

Reagents. $ClONO_2$ was synthesized by reacting N_2O_5 with Cl_2O as described by Davidson et al.[32] The $ClONO_2$ sample was purified via three vacuum distillations and further purified by pumping directly on the sample to remove more volatile impurities. The purity of the sample was checked by ultraviolet absorption and shown to have small impurities of Cl_2 (<10%) and Cl_2O (<1%). When not in use, the $ClONO_2$ sample was stored in the dark at 195 K. H_2O (>99.9%) was purified via several freeze−pump−thaw cycles before use.

$ClONO_2$ was introduced to the reactor by flowing vapor off a bulk sample held at 225 K through a 12 in. glass tube and leak valve into the chamber. $ClONO_2$ and H_2O were flowed through separate leak valves to prevent the occurrence of heterogeneous conversion of $ClONO_2$ to HNO_3. The tube and leak valve were baked frequently to eliminate any H_2O or HNO_3 in the lines.

In the present study $ClONO_2$ was monitored in the chamber using mass spectrometry at mass/charge peaks 30, 35, 37, and 46. Monitoring parent masses 97 and 99 was not possible due to fragmentation produced in our high-energy electron-impact ionization source. The mass spectrometer signals (*m*/*z* 30, 35, 37, and 46) arising from $ClONO_2$ were linear with respect to $ClONO_2$ pressure as measured by a Baratron capacitance manometer and calibrated ionization gauge over the range of pressures used, $(5-100) \times 10^{-7}$ Torr. Thus, eq VIII was used without any corrections to convert mass spectrometer signals into relative $ClONO_2$ concentrations. Difficulties arising from the lack of any $ClONO_2$ parent peaks are described in the Discussion section. H_2O was monitored using mass peak *m*/*z* = 18 in combination with the Baratron capacitance manometer.

Results

$ClONO_2$ Deposition on Aluminum at 110 K. To further check the purity of our $ClONO_2$ source as well as to ensure that heterogeneous decomposition was not occurring in our inlet lines, solid films of $ClONO_2$ were grown on the aluminum substrate at 110 K. Figure 3A shows the spectrum obtained upon exposing the cold substrate to 5×10^{-6} Torr of $ClONO_2$ for ≈60 s. The base pressure of H_2O in our chamber ($\leq 5 \times 10^{-8}$ Torr) is sufficiently high that condensation of a small amount of H_2O is unavoidable at 110 K. Therefore, the spectrum in Figure 3A represents $ClONO_2$ deposited on a <5 nm thick water ice film. The thin H_2O ice film was ratioed out in the background, and thus water bands are not evident in the spectrum. The $ClONO_2$ spectrum obtained shows all five of the nine fundamental bands of $ClONO_2$ observable within the wavelength range of our detector. Peak positions for the various fundamentals are the NO_2 wagging mode (ν_8) at 715 cm^{-1}, the ONO scissors mode (ν_4) at 788 cm^{-1}, the ClO stretching mode (ν_3) at 829 cm^{-1}, the NO_2 symmetric stretch (ν_2) at 1303 cm^{-1}, and the NO_2 asymmetric stretching mode (ν_1) at 1700 cm^{-1}. Two weak absorption features were observed at 1450 and 2986 cm^{-1} which have been previously assigned to an overtone of the NO_2 wag and a combination ($\nu_6 + \nu_2$) band, respectively. The peak positions listed above are in excellent agreement with both matrix isolation data and previous reflection−absorption infrared studies.[18,33]

In addition to the $ClONO_2$ bands, a very weak feature at 966 cm^{-1} was observed due to infrared absorption of a small amount of HNO_3 impurity. We estimate the extent of this impurity to be <5% of the film from separate HNO_3 deposition experiments at 110 K. The source of this slight HNO_3 impurity was likely due to the reaction of $ClONO_2$ with condensed H_2O on the aluminum surface at 110 K or with H_2O on the walls of the gas handling lines. To investigate the source of the HNO_3 in our system, gas mixtures of $ClONO_2$ and H_2O were exposed to the aluminum surface at 110 K. In these experiments, the surface was first cooled to 110 K and isolated from the lower chamber. Next, $ClONO_2$ and H_2O were introduced into the lower chamber to establish a well-characterized gas mixture. Figure 3B shows the spectrum obtained upon dosing the surface with a gas mixture of 10:1 H_2O:$ClONO_2$ ($\{H_2O\} = 7 \times 10^{-6}$ Torr and $\{ClONO_2\} = 7 \times 10^{-7}$ Torr) for ≈60 s. The spectrum shown in Figure 3B is clearly different than that obtained from deposition of $ClONO_2$ alone (Figure 3A). As expected, the amorphous H_2O absorption features centered at ≈3370 and 850 cm^{-1} are now the most intense absorptions in the spectrum due to the excess of water vapor exposed to the cold substrate from our gas mixture. Slight absorptions in all the $ClONO_2$ fundamental modes at 1696, 1293, 830, and 780 cm^{-1} are noticeable. The appearance of several major new absorption features at 1450 and 1310 cm^{-1} (NO_3^-) and 1660 cm^{-1} (H_3O^+) are also apparent. These absorptions are attributed to generation of solvated HNO_3 from reaction 1. Upon turning off the flow of water into the chamber, the only change in spectra observed was a continual increase in the $ClONO_2$ fundamental absorption features. These experiments suggest HNO_3 formation from reaction 1 is possible even at 110 K, and thus, reaction 1 must proceed through a very low activation barrier. This conclusion is supported by recent theoretical studies.[16] Thus, we conclude that the slight HNO_3 impurity present in Figure 3A is likely a result of $ClONO_2$ reacting with water condensed on the Al substrate and not from reactions occurring in our inlet lines.

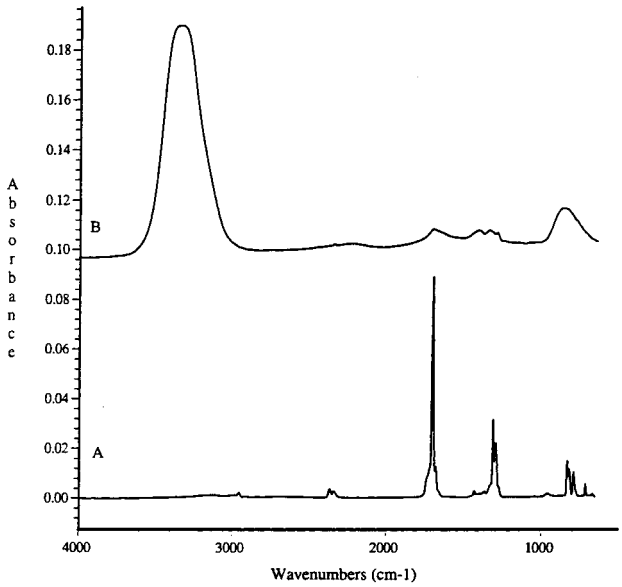

Figure 3. FTIR-RAS spectra of thin $ClONO_2$ and H_2O films at 110 K: (A) "pure" $ClONO_2$ and (B) $ClONO_2$ and H_2O (1 to 10 mole ratio).

$ClONO_2$ Reactions on NAD and NAT and at 185 K. Before determining the reaction efficiencies on NAD and NAT, we first characterized the loss of $ClONO_2$ on the stainless steel walls of the reactor in the absence of a PSC film. These expansions were performed over the range of flow rates investigated (flow = $(3.5-35) \times 10^{13}$ molecules s^{-1}). An example of the $ClONO_2$ temporal profile observed in such an expansion is shown in Figure 4A. In all cases the expansion was characterized by a rapid decrease upon opening the butterfly

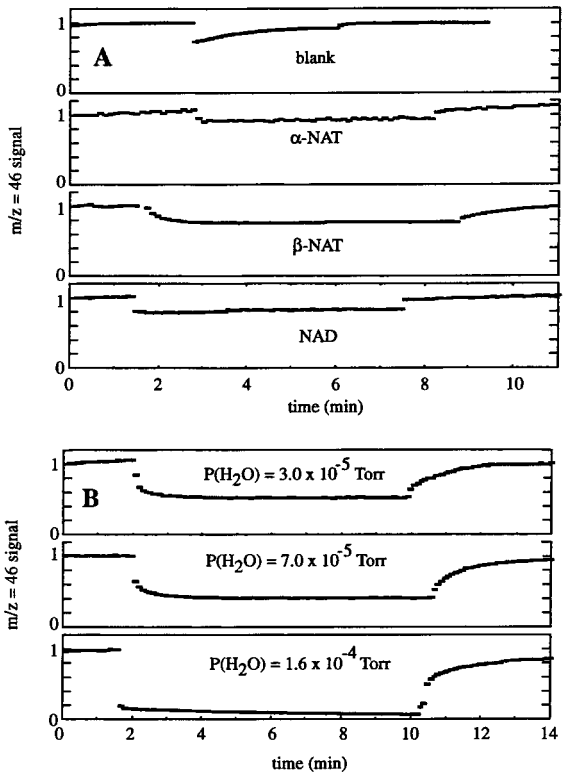

Figure 4. (A) Mass spectrometer traces ($m/z = 46$ (NO_2^+)) obtained with no ice present (blank) and upon exposing a flow of $ClONO_2$ to α-NAT, β-NAT, and NAD surfaces at a water partial pressure of 5×10^{-6} Torr (normalized to initial values of one for clarity). (B) Mass spectrometer traces obtained upon exposing a flow of chlorine nitrate to β-NAT at varying partial pressures of H_2O (normalized to initial values of one for clarity).

valve followed by a recovery to a value slightly below the original mass spectrometer signal. This indicates that the chamber walls did act as a sink for $ClONO_2$, and hence, the reaction efficiencies reported below were corrected for this additional loss process. The magnitude of the expansion recovery was very reproducible (±5%) and independent of $ClONO_2$ flow rate. Although highly reproducible, when measuring very small reaction probabilities ($\gamma < 0.001$) this correction introduced significant uncertainty.

The reaction efficiencies for reaction 1 on NAD and NAT surfaces at 185 K were measured over a range of relative humidities, and the condensed-phase products were observed as a function of time. Typically, reactant films were grown to a thickness exceeding 100 nm and slowly desorbed to the desired range of thickness (≈5−50 nm) by pumping directly on the film. α-NAT, β-NAT, and NAD each exhibits unique infrared spectra; therefore, identification of the reactant film composition was done by monitoring the spectrum of the film upon crystallization. After achieving the desired film composition (NAT or NAD) and thickness, the gate valve was shut so that pumping occurred via effusion through the 0.17 cm^2 hole. Under these conditions, the reactant NAD and NAT films were stable over the course of an experiment.

After preparing a stable NAD or NAT film in the upper chamber, the reactant film was isolated from the lower chamber by closing the butterfly valve between the upper and lower chambers. A steady flow of $ClONO_2$ was introduced to the lower chamber to attain a partial pressure of 1×10^{-6} Torr and monitored by the $m/z = 30$ (NO^+), $m/z = 35$ (Cl^+), $m/z = 37$ (Cl^+), and $m/z = 46$ (NO_2^+) signals from the mass spectrometer. An additional flow of H_2O was introduced to the lower chamber to obtain a total chamber pressure in the range $(0.5-20) \times 10^{-5}$ Torr.

When the flows of $ClONO_2$ and H_2O had stabilized, the butterfly valve was opened, and the flows of $ClONO_2$ and H_2O were exposed to the reactant NAD or NAT film. In all cases, significant drops in the $m/z = 30$, 35, 37, and 46 signals occurred upon opening the valve, after which the signals remained essentially constant. When the valve was closed, the signals recovered to their previous values before opening. Identical behavior was observed upon opening and closing the butterfly valve a second time. Figure 4A shows $m/z = 46$ (NO_2^+) traces for the exposure of $ClONO_2$ to ≈20 nm thick NAD, α-NAT, and β-NAT films in the presence of $\approx 5 \times 10^{-6}$ Torr of H_2O.

The observed decrease in mass spectrometer signals results from $ClONO_2$ reacting with the hydrate surface. Therefore, $ClONO_2$ mass spectrometer signals before (I_0) and after (I) exposure to the surface undergoing reaction can be related to the reaction efficiency for reaction 1 by eq VIII. Using $A_s = 72$ cm^2 as the geometric surface area of the aluminum substrate (including a 6.4 cm^2 contribution from the edge), the $m/z = 46$ (NO_2^+) and $m/z = 30$ (NO^+) signals yielded an average reaction efficiency for reaction 1 on NAD of $\gamma = (5 \pm 3) \times 10^{-4}$ for conditions of 5×10^{-6} Torr of H_2O. Experiments probing the reactivity of α- and β-NAT surfaces for conditions of 5×10^{-6} Torr of H_2O yielded similar reaction efficiencies of γ(β-NAT) $= (5 \pm 3) \times 10^{-4}$ and γ(α-NAT) $= (4 \pm 2) \times 10^{-4}$. Using $ClONO_2$ fragments $m/z = 35$ and 37 ($^{35}Cl^+$ and $^{37}Cl^+$) yielded values of γ approximately 30% smaller than those determined using m/z 46 and 30 for measurements on both NAD and NAT surfaces. An explanation for this discrepancy follows in the Discussion section.

The reaction efficiencies for $ClONO_2$ on NAD and NAT surfaces were measured over a wide range of water partial pressures ($5 \times 10^{-6}-2.0 \times 10^{-4}$ Torr). To ensure that each $ClONO_2$ expansion was interacting with a clean acid hydrate surface, the reactant film was directly pumped on after each exposure. The magnitude of the reaction efficiency for reaction 1 on NAD, α-NAT, and β-NAT surfaces was observed to increase systematically as the partial pressure of H_2O was increased. Figure 4B shows mass spectrometer traces ($m/z = 46$ (NO_2^+)) for exposure of an approximately 20 nm thick β-NAT film to 1×10^{-6} Torr of $ClONO_2$ and water partial pressures ranging from 3×10^{-5} to 1.6×10^{-4} Torr. Using eq VIII, reaction efficiencies were determined to range from $\gamma = 0.0004$ to $\gamma = 0.007$ as the water partial pressure was increased from 5×10^{-6} to 1.4×10^{-4} Torr at 185 K. Again, mass spectrometer signals $m/z = 35$ ($^{35}Cl^+$) and 37 ($^{37}Cl^+$) yielded values of γ that were ≈30% smaller than those determined using $m/z = 46$ and 30 for all water partial pressures investigated. As discussed below, we prefer to report values of γ obtained from mass signal $m/z = 46$ (NO_2^+). Figure 5A summarizes all the measurements of γ as a function of H_2O partial pressure at 185 K for both NAT and NAD reactant films.

The values of the reaction efficiency obtained in the present study for reaction 1 were observed to be independent of the $ClONO_2$ concentration ($(1-10) \times 10^{-6}$ Torr) exposed to the reactant NAD or NAT film. In addition, the measured reaction efficiencies did not change significantly upon switching the substrate material from aluminum to gold or varying the thickness of the reactant NAD and NAT films between ≈5 and 50 nm.

The composition of the reactant NAD and NAT films was monitored before, during, and after exposure to $ClONO_2$. Exposure of thin NAT and NAD films to $ClONO_2$ in the presence of water ($P_{H_2O} \geq 4 \times 10^{-5}$ Torr) always resulted in continuous growth of the reactant film as indicated by increased total integrated absorbance of the FTIR-RAS spectra of the thin

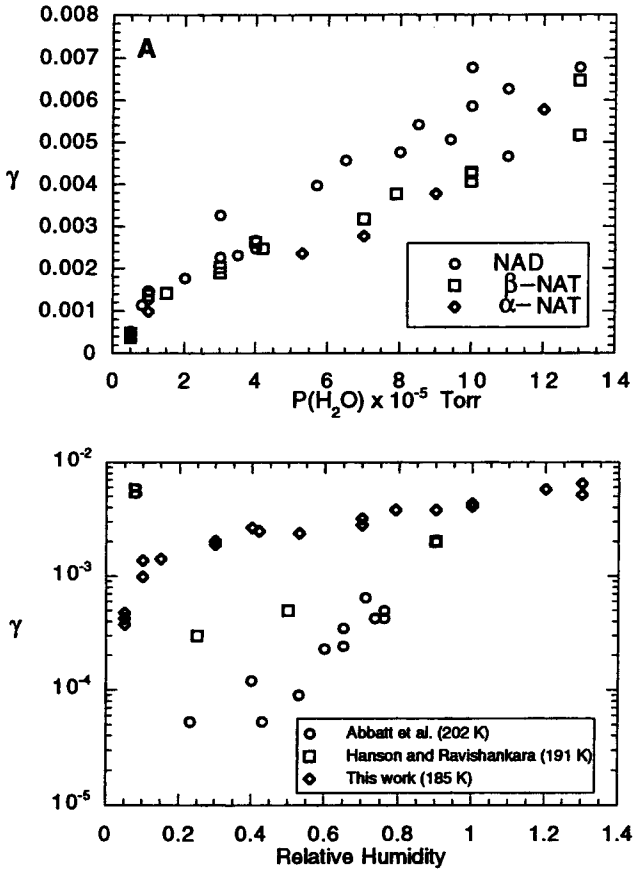

Figure 5. Summary of the reaction efficiencies measured in the present study. (A) The reaction efficiencies measured on NAD, α-NAT, and β-NAT surfaces plotted on a linear scale. (B) A comparison of our NAT results with measurements from previous studies at higher temperatures plotted on a logarithmic scale.

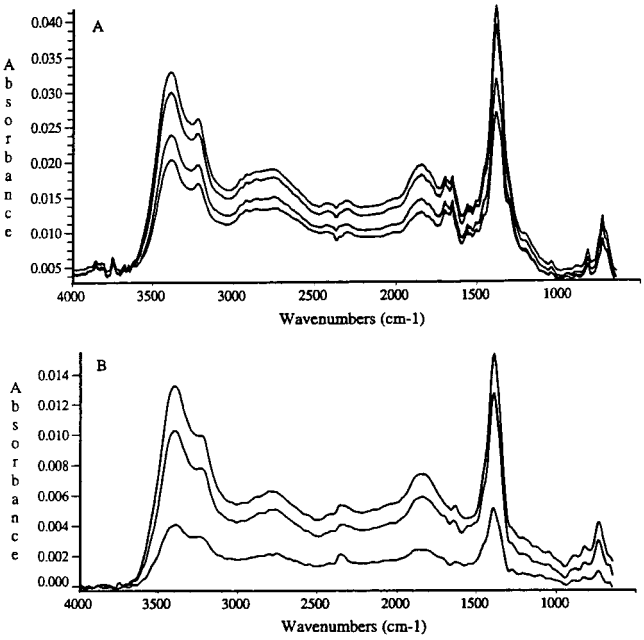

Figure 6. FTIR-RAS spectra obtained upon exposing a β-NAT film to 6×10^{-6} Torr of $ClONO_2$ and 8×10^{-5} Torr of H_2O: (A) spectra as a function of time with the lower spectrum taken at 0 min and the upper spectra taken at 4, 7, and 13 min; (B) subtractions at $t = 4$, 7, and 13 min.

reacting films. For example, Figure 6A shows the infrared spectra observed during exposure of a thin NAT film to 6×10^{-6} Torr of $ClONO_2$ and 8×10^{-5} Torr of H_2O. Subtraction spectra are shown in Figure 6B to highlight the changes that

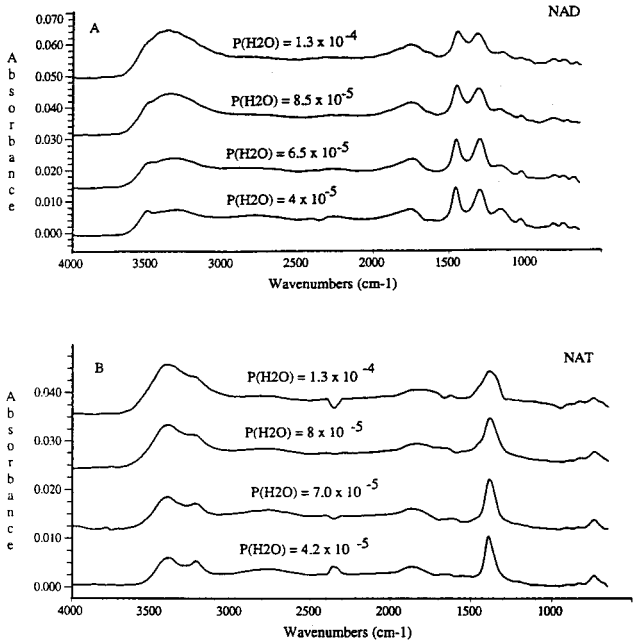

Figure 7. Product FTIR-RAS spectra (subtractions) obtained upon exposing a ≈20 nm thick reactant (A) NAD film and (B) β-NAT film to $ClONO_2$ and varying H_2O partial pressures.

occurred due to reaction. In the subtraction it is clear that there is increased absorption in all the major β-NAT absorption bands (3380, 3228, 1851, 1394, and 825 cm^{-1}) upon exposure to $ClONO_2$ and H_2O. Increased absorption in the β-NAT absorptions can be attributed to HNO_3 production from reaction 1 and subsequent incorporation into the NAT crystal structure. In addition to NAT absorptions, a new broad absorption feature centered at 3370 cm^{-1} is apparent on close examination of the subtraction spectra. The broad absorption feature observed at 3370 cm^{-1} is likely due to the presence of surface-absorbed water not incorporated into the NAT lattice structure. Below we will show that this water is probably contained in an aqueous HNO_3 surface layer on NAT.

NAD films also exhibited a significant change in their FTIR-RAS spectra after being exposed to $ClONO_2$ and H_2O. Subtraction spectra revealed similar behavior as that observed for experiments for β-NAT. The product spectra observed were characterized by growth in the major NAD absorption features (3496, 3267, 1756, 1461, 1307, and 803 cm^{-1}), indicating HNO_3 production from reaction 1 and incorporation into the hydrate lattice. In addition, a broad absorption feature at 3370 cm^{-1} was again noticeable in the product spectra due to water in the surface layers.

Subtraction spectra for investigations of reaction 1 on NAD and NAT were obtained for exposure times up to 15 min. Comparison of the subtraction spectra at successive time intervals for a constant H_2O partial pressure revealed that the product layers possessed essentially constant composition during the 15 min exposure. However, the composition attained varied as the H_2O partial pressure was changed.

Figure 7 (A and B) shows the product spectra observed upon exposing ≈20 nm thick NAD and β-NAT films to $ClONO_2$ and H_2O for a variety of water partial pressures. As shown in this figure, the product spectra observed for conditions of low water partial pressures ($P_{H_2O} \leq 5 \times 10^{-5}$ Torr) are nearly indistinguishable from the initial reactant NAD and NAT films. However, at higher partial pressures of H_2O the magnitude of the broad absorption centered at 3370 cm^{-1} increased relative to the nitrate feature at ~1400 cm^{-1}. Subtractions indicate that the feature at 3370 cm^{-1} is attributable to surface-adsorbed water not incorporated into the hydrate lattice. The variation in

subtraction spectra for different water partial pressures suggests that the amount of "free" water on the reaction surface increased systematically with water pressure.

Product spectra similar to those shown in Figure 7 were also acquired for investigations of reaction 1 on α-NAT surfaces. As mentioned previously, at 185 K α-NAT spontaneously converted to β-NAT throughout the course of an experiment. Exposure of $ClONO_2$ and H_2O to α-NAT films yielded product spectra characterized by an absorption centered at 3370 cm^{-1} in addition to the α-NAT and β-NAT fundamental absorptions. As in the case of experiments on β-NAT and NAD films, the intensity of the absorption at 3370 cm^{-1} was observed to increase as the H_2O partial pressure above the reactant film was increased.

As shown in Figures 6 and 7, upon exposing $ClONO_2$ to NAD and NAT films, no absorption features attributable to molecular HOCl were observed in the condensed-phase products at 185 K. These observations suggests that HOCl, the coproduct of reaction 1, rapidly desorbs from the NAD and NAT surfaces at 185 K and, hence, did not accumulate significantly on the reactant surface.

At high H_2O partial pressures ($P_{H_2O} \geq 1.0 \times 10^{-4}$ Torr), product adlayers from reaction 1 on NAD and NAT films possessed HNO_3 vapor pressures significantly larger than that of the initial reactant films. Under these conditions, infrared spectra of the product films indicated rapid loss of adlayers upon lowering the pressure of water in the chamber. After isothermal desorption of the product layers, the original NAD or NAT infrared spectrum was easily regained. Once the product adlayers had desorbed, the reflection−absorption spectrum of the film remained essentially constant, and the pressure inside the chamber decreased significantly. These observations indicate that the observed product layers at high water partial pressures were likely composed of a metastable HNO_3/H_2O phase such as an aqueous HNO_3 solution.

The rate of condensed-phase product growth, resulting from reaction 1, increased as the partial pressure of $ClONO_2$ ((1−10) × 10^{-6} Torr) exposed to the NAD and NAT reactant film was raised. Despite the dependence of the product growth rate on the partial pressure of $ClONO_2$ in the chamber, the spectra of growing adlayers at a given water partial pressure were essentially identical for the entire range of $ClONO_2$ partial pressures used. Obtained product spectra did not vary upon changing the thickness (≈20−50 nm) of the reactant hydrate film or substrate material (Al or gold).

Ice Nucleation and Growth on NAD and NAT. Reaction 1 on NAT and NAD surfaces was also studied under water partial pressures at and above the ice frost point at 185 K (frost point at 185 K = 1.03×10^{-4} Torr).[34] Ice nucleation was not observed on NAT and NAD for H_2O partial pressures $< 1.5 \times 10^{-4}$ Torr. Rather, as shown in Figure 7, water-rich surface layers were observed for both NAT and NAD reactant films for partial pressures of $H_2O < 1.5 \times 10^{-4}$ Torr. As discussed below, we attribute the product spectra to the formation product adlayers composed of aqueous HNO_3 solutions in coexistence with NAT or NAD.

At water partial pressures above 1.5×10^{-4} Torr, exposure of $ClONO_2$ to NAT and NAD films resulted in noticeable changes in the FTIR-RAS product spectra. These changes were characterized by the rapid appearance of a sharp absorption feature at 3220 cm^{-1} and a broad feature centered at 850 cm^{-1}. Figure 8 shows the spectrum obtained from exposing a β-NAT film to 3×10^{-6} Torr of $ClONO_2$ and 1.6×10^{-4} Torr of H_2O. The appearance of the new absorption features at 3220 and 850 cm^{-1} may be attributed to the nucleation and growth of hexagonal water ice on top of the reactant NAT film.[24,29] The

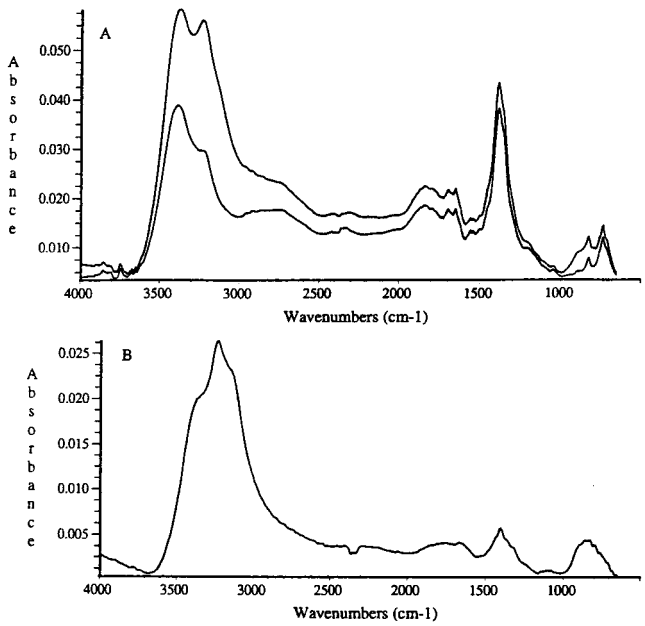

Figure 8. FTIR-RAS spectra observed upon exposing 3×10^{-6} Torr of $ClONO_2$ and 1.6×10^{-4} Torr of H_2O to a β-NAT reactant film. (A) is the observed spectra at $t = 0$ and 2 min and (B) is subtraction after 2 min.

subtraction spectrum shown in Figure 8B is in excellent agreement with previous FTIR-RAS spectra of crystalline water ice.[35] Nucleation of ice on NAD was also observed at water pressures greater than 1.5×10^{-4} Torr.

The subtraction spectrum in Figure 8B also reveals a slight increase in absorption at ≈1400 cm^{-1}. This is indicative of growth of NAT prior to and during ice nucleation. The uptake of $ClONO_2$ was also monitored for experiments using water partial pressures $> 1.5 \times 10^{-4}$ Torr. Figure 4B includes a mass spectrometer trace for conditions in which $ClONO_2$ (1×10^{-6} Torr) and H_2O (1.6×10^{-4} Torr) were exposed to a NAT film at 185 K. The decrease in all $ClONO_2$ mass spectrometer signals for experiments on both NAT and NAD indicated that the reaction efficiencies increased significantly under conditions of ice nucleation and growth. The reaction efficiency for reaction 1 under these conditions was determined to exceed the limit that we can measure accurately. Therefore, we report a lower limit on the reaction efficiency of reaction 1 on ice of $\gamma_{ice} > 0.02$.

Discussion

Reaction Efficiency for Reaction 1. In the present study, $ClONO_2$ could only be detected by fragment peaks 30 (NO^+), 35 (Cl^+), 37 (Cl^+), and 46 (NO_2^+) due to the very energetic nature of our electron ionizer. This makes measurement of the uptake coefficient for reaction 1 difficult because the products of this reaction, HOCl and HNO_3, are also likely to fragment to identical mass peaks. Our measurements of γ for reaction 1 using peaks 35 and 37 were systematically smaller (30%) than those determined using masses 30 and 46. This is likely due to interferences arising from HOCl formation and subsequent desorption from the nitric acid hydrate surface. Indeed, no HOCl was observed in the FTIR-RAS product spectra upon exposing $ClONO_2$ to NAT or NAD films. This observation strongly suggests that HOCl desorbs rapidly upon formation at 185 K. No parent mass was observed for HOCl in our mass spectrometer; therefore, it is likely to have fragmented producing masses 35 and 37. This would lead to an enhancement in the mass spectrometer signals of masses 35 and 37 upon exposing $ClONO_2$ to the reactant surface and interfere with the determination of γ for reaction 1.

Upon exposing $ClONO_2$ to reactant acid hydrate films, slow growth of the NAT and NAD absorption features was always observed. This suggests that, in contrast to HOCl, HNO_3 produced from reaction 1 is permanently incorporated into the hydrate surface upon formation. Therefore, HNO_3 formation should not interfere with the determination of γ from masses 46 and 30. The $ClONO_2$ signals at masses 30 and 46 were of similar magnitude. In contrast, the HNO_3 signal at mass 30 was approximately 1 order of magnitude larger than that at mass 46. Although we do not think HNO_3 formation from reaction 1 interfered significantly with our measurements, we only report values of γ for reaction 1 determined using mass 46.

As in previous studies, we find that the reaction efficiency for reaction 1 on NAT increases with increasing relative humidity.[5,6] The values we obtain at 185 K can be compared to those found earlier at higher temperatures. Our studies were limited to temperatures $\leqslant$185 K because at higher temperatures desorption is fast enough to significantly reduce the lifetimes of our thin acid hydrate films upon closing the butterfly valve. Abbatt and Molina report $\gamma = 0.002 \pm 0.001$ for reaction 1 on NAT under conditions of 88% relative humidity at 202 K.[5] Hanson and Ravishankara report an identical value of $\gamma = 0.002$ at 90% relative humidity and 191 K.[6] These previous measurements agree reasonably well with our slightly higher value of $\gamma = 0.004 \pm 0.002$ at 185 K and 90% relative humidity. A standard propagation of errors in A_h (8%), A_s (3%), I (5%), and I_0 (5%) yielded an error in γ of $\pm$10%. However, the reproducibility of an experiment generally resulted in a much larger error of $\pm$50%.

Although our measurement of the reaction efficiency for reaction 1 on NAT surfaces at a relative humidity of 90% agrees with previous work, values of γ deviate significantly at lower relative humidities. Figure 5B displays a collection of measurements of the reaction efficiency for $ClONO_2$ on NAT as a function of relative humidity. It should be noted that in Figure 5B relative humidity is determined relative to the water vapor pressure over ice at the various temperatures studied. Therefore, for the same relative humidity the actual water partial pressures of the three studies differed considerably. The plot clearly shows that experiments performed by Abbatt and Molina at 202 K result in a much steeper dependence on relative humidity than the current results observed at 185 K. The values at 190 K from Hanson and Ravishankara show intermediate behavior.[5,6]

As suggested by our 110 K codeposition results, reaction 1 is likely to proceed through a very low activation barrier. Therefore, any temperature dependence in the reaction efficiency of reaction 1 on NAT is likely to arise from changes in the surface coverage of water for identical relative humidities at different temperatures. Using a physical adsorption model constrained by parameters from experiment, Henson et al. have modeled reaction 1 on both NAT and SAT surfaces.[16] In this model the temperature dependence of the H_2O surface coverage is assumed to scale with the vapor pressure of water ice. Henson et al. are able to reproduce the results of Abbatt et al. extremely well; however, the calculations are significantly lower than the efficiencies measured by Hanson and Ravishankara and in the present study. In addition, although the model of Henson et al. was able to reproduce the temperature dependence of reaction 1 on SAT as measured by Zhang et al.,[9] the results of Hanson and Ravishankara[6] on SAT at low relative humidity (high temperatures) significantly deviate from the model predictions. Thus, it is possible that the temperature dependence of the vapor pressure of ice may not adequately describe the temperature dependence of the adsorption and desorption kinetics of H_2O on hydrate surfaces. This is especially valid considering the fact that ice nucleation on NAT was not even observed for water partial pressures at the frost point. Direct measurements of the H_2O adsorption and desorption rate coefficients on NAT as a function of temperature may prove useful in resolving the exact nature of the overall temperature dependence of reaction 1 on NAT.

Another possible explanation of the discrepancies noted above involves the morphology of the NAT films used in the present and previous studies. The roughness of laboratory ice films has been an unresolved controversy in the literature for the past 5 years.[36,37] The preparation methods employed in the present study differ considerably from those used previously by Abbatt et al. and Hanson and Ravishankara.[5,6] The films of Abbatt et al. and Hanson and Ravishankara were prepared by vapor deposition of ice at 202 and 191 K, respectively, followed by exposure to HNO_3 for approximately 1 h. In the present study NAT films were primarily prepared by codeposition at 150 K followed by annealing. Previous work by Middlebrook et al. has shown that NAT prepared by this latter process results in considerably flatter films than those prepared by direct deposition.[38] In addition, the present films were very thin (5−50 nm) and would thus be unlikely to develop as much roughness as thicker films. These factors suggest that the films used in the present study were, if anything, more smooth than those employed in previous studies. In addition, we note that no systematic change in the magnitude of γ was observed upon changing the thickness of our NAT reactant film from 5 to 50 nm. This implies that the use of geometric surface area in eq VIII is valid. However, because none of these studies measured the actual surface area during reaction, we cannot completely eliminate the possibility that the temperature dependence we suggest for reaction 1 is really a manifestation of morphology differences in the NAT films.

In addition to factors such as temperature and surface morphology, the presence of contaminants such as HNO_3 in the $ClONO_2$ source used in the present study could also contribute to the observed discrepancies because m/z 46 is a fragmentation product of both $ClONO_2$ and HNO_3. HNO_3 has a large accommodation coefficient on NAT ($\alpha = 0.3$) at 100% relative humidity.[39] Although much lower uptake of HNO_3 is observed on NAT at lower relative humidity,[39] exact values of the accommodation coefficients on NAT are not available as a function of relative humidity. Thus, a large HNO_3 contaminant in the $ClONO_2$ source could potentially lead to an erroneously high value of γ for reaction 1. However, our FTIR-RAS spectra of "pure" $ClONO_2$ suggest that we indeed used a very pure source, and thus this is unlikely to be the cause of the discrepancy. Thus, we conclude that the most likely explanation for the differences in the observed γ values for reaction 1 is the different temperatures used in the three studies.

The reactivity of NAD films was also investigated as a function of relative humidity at 185 K. In our experiments the exact stoichiometry of the reactant hydrate film before, during, and after exposure to $ClONO_2$ is directly monitored via reflection−absorption infrared spectroscopy. Thus, we are confident of the exact composition of the reactant NAD film over the entire duration of the measurement. The reactivity of NAD with $ClONO_2$ was observed to be quantitatively very similar to that on NAT surfaces. The similarity of $ClONO_2$ reactivity on NAT and NAD surfaces is likely to arise from the reaction occurring on water absorbed on the hydrate surface and not on the "neat" hydrate surface alone. This argument would explain why the reactivity of HNO_3 hydrate films is independent of hydrate stoichiometry. Hanson and Ravishankara also report that the reactivities of NAT and NAD are similar; however, they mention that their NAD films were metastable throughout the course of an experiment and slowly

converted to NAT.[6] In contrast, the NAD films used in our experiments were observed to be stable for the entire course of an experiment and could be easily regained after reaction by pumping directly on the film. The present measurements of the rate of reaction 1 on NAD imply that, in the atmosphere, NAD surfaces are likely to be as reactive as NAT surfaces and will follow a similar relative humidity and temperature dependence.

A recent thermodynamic modeling study of $ClONO_2$ interacting with NAT surfaces has also suggested that the availability of surface-absorbed water ultimately governs the rate of reaction 1.[16] Although we cannot quantify the surface water coverage on our thin reactant hydrate films, our results strongly suggest that the surface water content of the reactant film plays a primary role in determining the rates of reaction 1 on NAD and NAT. A similar modeling treatment of NAD would be interesting in light of the present results.

Identification of Condensed-Phase Products. The product spectra observed during reaction yield insight into the mechanism and relative humidity dependence of reaction 1 on NAT and NAD surfaces. In the present study HNO_3 formed from reaction 1 was found to be retained in the condensed phase as shown by the growth of the reactant hydrate film. However, the composition of the surface layer governing the reaction kinetics was observed to depend on the partial pressure of H_2O above the hydrate surface. At low relative humidities, $P < 5 \times 10^{-5}$ Torr, NAT or NAD surface layers were formed that possessed an infrared spectrum nearly indistinguishable from the original reactant film. In contrast, for water partial pressures $>5 \times 10^{-5}$ Torr, the spectra of the condensed-phase products reveal an additional absorption centered at 3370 cm^{-1} not present in the spectrum of the original crystalline hydrate film. Previous FTIR-RAS studies of thin amorphous H_2O ice films have shown that the OH stretch is primarily characterized by a broad absorption band centered around $\nu \approx 3370$ cm^{-1} and a smaller feature at $\nu \approx 850$ cm^{-1} corresponding to the H_2O libration.[35] The spectra of the water-rich surface layers on NAT and NAD did not possess significant absorption at 850 cm^{-1} corresponding to the H_2O libration in supercooled water. This suggests that there are no long-range water−water interactions, either due to perturbations from the hydrate environment or due to solvation of extra HNO_3 not incorporated into the bulk. Considering the $ClONO_2$ flow into the chamber acts as a continuous source of HNO_3 to the reactant film, it is very likely that the aqueous solution observed at the surface contained some solvated nitric acid.

To gain a more quantitative understanding of the thin water-rich hydrate films observed in the present study, reference NAT and NAD spectra were subtracted from the product spectra observed at high relative humidities. In these subtractions a scaling factor was used to minimize the absorption in the NAT and NAD fundamental bands. The results of such an analysis are shown in Figure 9 for the most water-rich surface layer shown in Figure 7. The obtained residual spectra are similar for both NAD and NAT surface layers and closely resemble previously reported FTIR-RAS spectra for amorphous HNO_3/H_2O with a composition of roughly 5:1 H_2O:HNO_3.[23,24] However, in the present case the HNO_3/H_2O layers are likely aqueous solutions since the experimental temperature of 185 K is well above the glass temperature of HNO_3/H_2O mixtures of ∼150 K.[40] Similar spectra were obtained for water-rich product spectra at different relative humidities and were primarily characterized by a broad absorption centered at ≈3300 cm^{-1} and two sharper features 1450 and 1310 cm^{-1}. However, product spectra taken at lower relative humidities revealed a decreased water content as indicated by a decrease in the ratio of the 3300

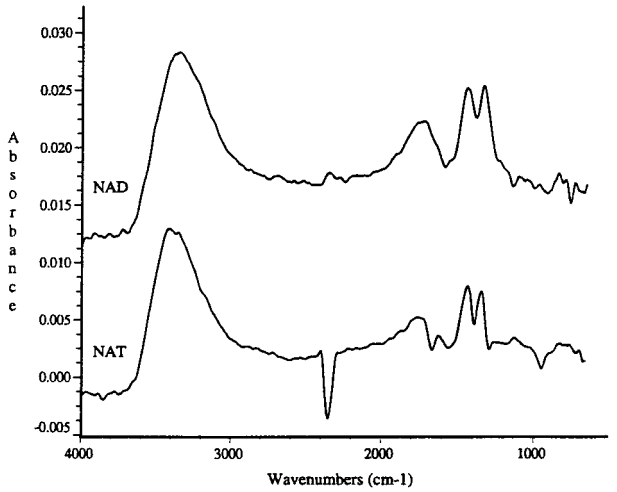

Figure 9. Residual spectra resulting from subtraction of NAD (A) and NAT (B) reference spectra from the most water-rich spectra shown in Figure 7, A and B, respectively.

to 1450 (and 1310) cm^{-1} bands.[23] Thus, it is very likely that the water-rich surface layers observed in the present study are composed of a layered product consisting of growing crystalline hydrate and an aqueous HNO_3/H_2O surface layer. Other surface probes such as scanning tunneling microscopy, atomic force microscopy, and second harmonic generation may prove useful in determining the exact nature of the water-rich forms of NAT and NAD observed in the present study.

Product spectra taken at exposure time intervals up to 15 min suggested that the growing adlayers possessed a constant composition for a constant water partial pressure. Also supporting this conclusion, the γ for reaction 1 on NAT and NAD was observed to be constant for reaction times up to 15 min. Together these observations support a mechanism of surface growth via a flux of both gas-phase HNO_3 (from reaction 1) and water to the hydrate surface. Ultimately, this mechanism results in a constant replenishment of water available for reaction leading to unlimited uptake of a constant efficiency.

Nucleation and Growth of Crystalline Water Ice. Crystalline ice nucleation and growth from the aqueous HNO_3 surface layer on top of the reactant NAD and NAT reactant films were only observed at saturation ratios $S \geq 1.5$. In our system we cannot determine whether ice nucleation occurred heterogeneously on the reactant acid hydrate surface or homogeneously from the aqueous HNO_3/H_2O surface layer. The saturation requirement ($S \geq 1.5$) measured in the present study suggests that a significant barrier exists for ice nucleation. This may indicate that the lattice structures of NAT and NAD are not optimally arranged to facilitate growth of the crystalline water ice lattice. Such lattice mismatching has been reported for solid/solid nucleation on other PSC surfaces.[41] If occurring homogeneously, the results of the present study suggest that a supercooling of H_2O/HNO_3 solutions to ≈2 K below the ice frost point is required for ice nucleation. This value was determined by relating the H_2O partial pressure over the thin film when ice nucleation was observed to a temperature using the equilibrium ice frost point data of Marti and Mauersberger.[34] This requirement is consistent with the predictions of current thermochemical models of homogeneous nucleation in the atmosphere. Indeed, the results of recent homogeneous nucleation calculations predict a similar saturation requirement for homogeneous nucleation of ice from aqueous sulfate solutions.[42] Regardless of the exact mechanism of nucleation (heterogeneous or homogeneous nucleation), the results of the present study suggest that ice nucleation in the atmosphere on NAT or NAD

particles at 185 K will only occur when water vapor pressures exceed a saturation ratio of $S = 1.5$.

Atmospheric Implications. The results of the present study suggest that atmospheric processing of $ClONO_2$ on crystalline type 1a PSCs is controlled largely by the amount of water adsorbed on to the particle surface and not by the stoichiometry of the HNO_3 crystalline hydrate. Our results predict that the availability of surface water is determined by the gas-phase partial pressure of H_2O and the temperature. HOCl was not observed as a condensed-phase product for reaction 1; thus, the present study supports previous work showing that the HOCl formed will be liberated into the gas phase where it can perturb chlorine levels.[3,7,36] In contrast, HNO_3 was observed to be efficiently incorporated into the reaction surface. Therefore, reaction 1 will also represent a significant sink for NO_y in the polar stratosphere.

Atmospheric particulate are constantly experiencing a variety of different H_2O partial pressures and temperatures. Thus, it is very likely that the metastable forms observed in the present study will also occur in the atmosphere. Hydrates other than those investigated in the present study are also likely to possess similar metastable reactive surface layers. For example, the reactivity of $ClONO_2$ on sulfuric acid tetrahydrate (SAT) has been shown to depend on the partial pressure of H_2O,[6,9] and it has been suggested to proceed through a similar physical adsorption mechanism.[16]

The exact composition of PSCs is currently unclear; however, field observations of PSCs suggest that both solid (type 1a) and liquid (type 1b) HNO_3-containing particles are formed in the atmosphere at temperatures above those required for ice nucleation.[43,44] Large discrepancies arise when the vapor pressures and water content of such solid type 1 PSCs observed in field are compared to the stable HNO_3 hydrates used in laboratory studies.[44−46] Indeed, field measurements of vapor pressures and volumes of atmospheric particulate suggest solid HNO_3 PSCs often consist of metastable solid particles with a greater water content than NAT and NAD.[47] This conclusion is also supported by infrared spectra of type 1 PSCs observed in the field.[48] Although the water-rich layers observed in our study were metastable, it is possible that significant amounts of water-rich multilayers of NAT or NAD can be formed in the atmosphere. This is especially the case for relative humidities >100% where metastable aqueous HNO_3/H_2O multilayers are likely to form. Thus, the water-rich NAT and NAD forms identified in the present study may prove helpful in explaining the complex nature of PSCs as observed in the field. Finally, our studies of ice nucleation on NAT and NAD suggest that type II PSC formation by this mechanism may require supercooling by 2 K below the frost point.

Acknowledgment. M.A.Z. acknowledges support from a NASA Global Change Fellowship and a NASA Earth System Science Fellowship. M.A.T. acknowledges support as an NSF Young Investigator and a Camille Dreyfus teacher−scholar. We also thank A. Tabazadeh, E. Jensen, and O. B. Toon for providing us with preprints of their work on homogeneous nucleation. Three anonymous reviewers are thanked for helpful comments. This research was funded by NSF Grant ATM-9321582 and NASA Grant SASS-94-091.

References and Notes

(1) Solomon, S. *Nature* **1990**, *347*, 347.
(2) Fahey, D. W.; Kawa, S. R.; Woodbridge, E. L.; Tin, P.; Wilson, J. C.; Jonsson, H. H.; Dye, J. E.; Baumgartner, D.; Borrmann, S.; Toohey, D. W.; Avallone, L. M.; Proffitt, M. H.; Margitan, J.; Loewenstein, M.; Podolske, J. R.; Salawitch, R. J.; Wofsy, S. C.; Ko, M. K. W.; Anderson, D. E.; Schoeberl, M. R.; Chan, K. R. *Nature* **1993**, *363*, 509.
(3) Molina, M. J.; Tso, T. L.; Molina, L. T.; Wang, F. C. Y. *Science* **1987**, *238*, 1253.
(4) World Meterological Organization WMO, Scientific Assessment of Ozone Depletion, 1994.
(5) Abbatt, J. P.; Molina, M. J. *J. Phys. Chem.* **1992**, *96*, 7674.
(6) Hanson, D. R.; Ravishankara, A. R. *J. Geophys. Res.* **1993**, *98*, 22931.
(7) Leu, M.-T. *Geophys. Res. Lett.* **1988**, *15*, 17.
(8) Tolbert, M. A.; Rossi, M. J.; Malhotra, R.; Golden, D. M. *Science* **1987**, *238*, 1258.
(9) Zhang, R.; Jayne, J. T.; Molina, M. J. *J. Phys. Chem.* **1994**, *98*, 867.
(10) Zhang, R.; Leu, M. T.; Keyser, L. F. *Geophys. Res. Lett.* **1995**, *22*, 1493.
(11) Robinson, G. N.; Worsnop, D. R.; Jayne, J. T.; Kolb, C. E.; Davidovits *J. Geophys. Res.* **1996**, *102*, 3583.
(12) Carslaw, K. S.; Luo, B. P.; Clegg, S. L.; Peter, T.; Brimblecombe, P.; Crutzen, P. J. *Geophys. Res. Lett.* **1994**, *21*, 2479.
(13) Hanson, D. R.; Ravishankara, A. R. *J. Geophys. Res.* **1991**, *96*, 5081.
(14) Oppliger, R.; Allanic, A.; Rossi, M. J. *J. Phys. Chem. A* **1997**, *101*, 1903.
(15) Tabazadeh, A.; Turco, P. *J. Geophys. Res.* **1993**, *98*, 12.
(16) Henson, B. F.; Wilson, K. R.; Robinson, J. M. *Geophys. Res. Lett.* **1996**, *23*, 1021.
(17) Hanson, D. R. *J. Phys. Chem.* **1995**, *99*, 13059.
(18) Sodeau, J. R.; Horn, A. B.; Banham, S. F.; Koch, T. G. *J. Phys. Chem.* **1995**, *99*, 6258.
(19) Tabazadeh, A.; Turco, R. P.; Jacobson, M. Z. *J. Geophys. Res.* **1994**, *99*, 12.
(20) Tolbert, M. A.; Rossi, M. J.; Golden, D. M. *Geophys. Res. Lett.* **1988**, *15*, 847.
(21) Quinlan, M. A.; Reihs, C. M.; Goldan, D. M.; Tolbert, M. A. *J. Phys. Chem.* **1990**, *94*, 3255.
(22) Middlebrook, A. M.; Iraci, L. T.; Tolbert, M. A. *J. Geophys. Res.* **1993**, *98*, 474.
(23) Ritzhaupt, G.; Devlin, J. P. *J. Phys. Chem.* **1991**, *95*, 90.
(24) Koehler, B. G.; Middlebrook, A. M.; Tolbert, M. A. *J. Geophys. Res.* **1992**, *97*, 8065.
(25) Toon, O. B.; Tolbert, M. A.; Koehler, B. G.; Middlebrook, A. M.; Jordan, J. *J. Geophys. Res.* **1994**, *99*, 25631.
(26) Greenler, R. G. *J. Chem. Phys.* **1966**, *44*, 310.
(27) Richwine, L. J.; Clapp, M. L.; Miller, R. E. *Geophys. Res. Lett.* **1995**, *22*, 2625.
(28) Tisdale, R. T.; Tolbert, M. A.; Toon, O. B. To be submitted to *Geophys. Res. Lett.*
(29) Koch, T. G.; Banham, S. F.; Sodeau, J. R.; Horn, A. B.; McCoustra, M. R. S.; Chesters, M. A. *J. Geophys. Res.* **1997**, *102*, 1513.
(30) Eisenberg, D.; Kauzmann, W. *The Structure and Properties of Water*; New York, 1969.
(31) Brown, D. E.; George, S. M.; Huang, C.; Wong, E. K. L.; Rider, K. B.; Smith, R. S.; Kay, B. D. *J. Phys. Chem.* **1996**, *100*, 4988.
(32) Davidson, J. A.; Cantrell, C. A.; Shetter, R. E.; McDaniel, A. H.; Calvert, J. G. *J. Geophys. Res.* **1987**, *92*, 10921.
(33) DeSaxce, A.; Schriver, L. *Chem. Phys. Lett.* **1992**, *199*, 596.
(34) Marti, J.; Mauersberger, K. *Geophys. Res. Lett.* **1993**, *20*, 363.
(35) Horn, A. B.; Banham, S. F.; McCoustra, R. S. *J. Chem. Soc., Faraday Trans.* **1995**, *91*, 4005.
(36) Hanson, D. R.; Ravishankara, A. R. *J. Phys. Chem.* **1992**, *96*, 2682.
(37) Keyser, L. F.; Moore, S. B.; Leu, M.-T. *J. Phys. Chem.* **1991**, *95*, 5496.
(38) Middlebrook, A. M.; Berland, B. S.; George, S. M.; Tolbert, M. A. *J. Geophys. Res.* **1994**, *99*, 25.
(39) Hanson, D. R. *Geophys. Res. Lett.* **1992**, *19*, 2063.
(40) Ji, K. Ph.D. Thesis, L'Universite de Paris, 1994.
(41) Iraci, L. T.; Middlebrook, A. M.; Tolbert, M. A. *J. Geophys. Res.* **1995**, *100*, 20969.
(42) Tabazadeh, A.; Jensen, E.; Toon, O. B. Submitted to *J. Phys. Chem.*
(43) Toon, O. B.; Browell, E. V.; Kinne, S.; Jordan, J. *Geophys. Res. Lett.* **1990**, *17*, 393.
(44) Dye, J. E.; Baumgardner, D.; Gandrud, B. W.; Kawa, S. R.; Kelly, K. K.; Loewenstein, M.; Ferry, G. V.; Chan, K. R.; Gary, B. L. *J. Geophys. Res.* **1992**, *97*, 8015.
(45) Drdla, K.; Tabazadeh, A.; Turco, R. P.; Jacobson, M. Z.; Dye, J. E.; Twohy, C.; Baumgardner, D. *Geophys. Res. Lett.* **1994**, *21*, 2475.
(46) Dye, J. E.; Baumgardner, D.; Gandrud, B. W.; Drdla, K.; Barr, K.; Fahey, D. W.; Delnegro, L. A.; Tabazadeh, A.; Jonsson, H. H.; Wilson, J. C.; Loewenstein, M.; Podolske, J. R.; Chan, K. R. *Geophys. Res. Lett.* **1996**, *23*, 1913.
(47) Tabazadeh, A.; Toon, O. B. *J. Geophys. Res.* **1996**, *101*, 9071.
(48) Toon, O. B.; Tolbert, M. A. *Nature* **1995**, *375*, 218.